Article:
Pellegrini, E., Juyoux, P., von Velsen, J. et al. (6 more authors) (2024) Metal fluorides—multi-functional tools for the study of phosphoryl transfer enzymes, a practical guide. Structure, 32 (10). 1834-1846.e3. ISSN 0969-2126

https://doi.org/10.1016/j.str.2024.07.007

Structure

Resource

Metal fluorides—multi-functional tools for the study of phosphoryl transfer enzymes, a practical guide

Graphical abstract

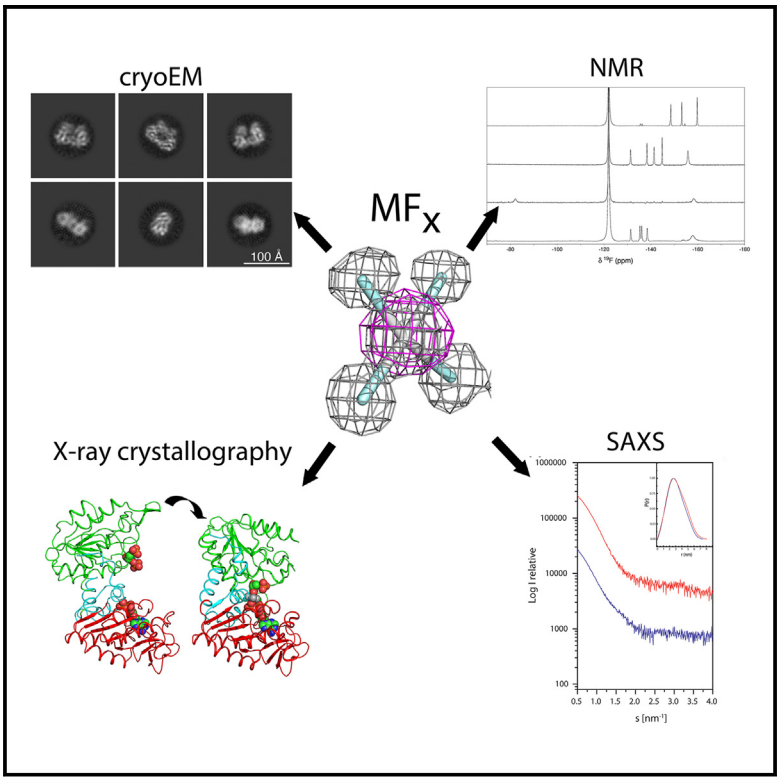

Authors

Erika Pellegrini, Pauline Juyoux, Jill von Velsen, ..., Matthew J. Cliff, Jonathan P. Waltho, Matthew W. Bowler

Correspondence

j.waltho@manchester.ac.uk (J.P.W.), mbowler@embl.fr (M.W.B.)

In brief

Metal fluorides mimic phosphate groups, stabilize active protein conformations, and are spectroscopically active. Pellegrini et al. present best practices for the formation and use of metal fluorides in the study of phosphoryl transfer proteins. They are useful in various techniques, including NMR, X-ray crystallography, cryo-EM, and SAXS.

Highlights

- Phosphoryl transfer enzymes have many crucial cellular functions
- Metal fluorides stabilize active conformations and are spectroscopically sensitive
- Metal fluorides mimic transition and ground states
- Guidelines for the formation of these complexes and their use are provided

Pellegrini et al., 2024, Structure *32*, 1–13
October 3, 2024
https://doi.org/10.1016/j.str.2024.07.007

CellPress

Structure

CellPress
OPEN ACCESS

Resource

Metal fluorides—multi-functional tools for the study of phosphoryl transfer enzymes, a practical guide

Erika Pellegrini,[1] Pauline Juyoux,[1] Jill von Velsen,[1] Nicola J. Baxter,[2] Hugh R.W. Dannatt,[2] Yi Jin,[2] Matthew J. Cliff,[3] Jonathan P. Waltho,[2,3,*] and Matthew W. Bowler[1,4,*]

[1]European Molecular Biology Laboratory, 71 avenue des Martyrs, CS 90181, 38042 Grenoble, France
[2]School of Biosciences, The University of Sheffield, Firth Court, Western Bank, Sheffield S10 2TN, UK
[3]Manchester Institute of Biotechnology, University of Manchester, Manchester M1 7DN, UK
[4]Lead contact
*Correspondence: j.waltho@manchester.ac.uk (J.P.W.), mbowler@embl.fr (M.W.B.)
https://doi.org/10.1016/j.str.2024.07.007

SUMMARY

Enzymes facilitating the transfer of phosphate groups constitute the most extensive protein families across all kingdoms of life. They make up approximately 10% of the proteins found in the human genome. Understanding the mechanisms by which enzymes catalyze these reactions is essential in characterizing the processes they regulate. Metal fluorides can be used as multifunctional tools to study these enzymes. These ionic species bear the same charge as phosphate and the transferring phosphoryl group and, in addition, allow the enzyme to be trapped in catalytically important states with spectroscopically sensitive atoms interacting directly with active site residues. The ionic nature of these phosphate surrogates also allows their removal and replacement with other analogs. Here, we describe the best practices to obtain these complexes, their use in NMR, X-ray crystallography, cryo-EM, and SAXS and describe a new metal fluoride, scandium tetrafluoride, which has significant anomalous signal using soft X-rays.

INTRODUCTION

Enzymes that catalyze phosphoryl transfer are the largest superfamily of enzymes and have roles in numerous crucial cellular functions. Understanding the methods that have evolved to enable the movement of phosphoryl groups is necessary to gain insight into many processes that it controls.[1,2] Metal fluoride moieties can occupy the active sites of phosphoryl transfer enzymes at the location of the transferring phosphoryl group and have been used to study these proteins by X-ray crystallography, cryogenic electron microscopy (cryo-EM), and NMR with excellent results. More recently, new metal fluoride complexes have been defined and characterized. Additionally, various other applications for these complexes have been discovered, expanding the toolkit accessible to scientists studying phosphoryl transfer enzymes.

Fluoride anions have been known for more than 50 years to modulate the activity of a range of phosphoryl transfer enzymes, such as kinases, phosphorylases, and phosphatases. However, the precise mechanism remained unknown until the discovery that millimolar concentrations of fluoride can leach aluminum cations from laboratory glassware. Aluminum and fluoride together, in the presence of guanosine diphosphate (GDP), were discovered to stimulate the activity of small G proteins.[3] Upon the solution of the structure at 1.7 Å of transducin α in 1994,[4] the nature of the species was confirmed as AlF_4^-, where it was shown to mimic the transition state of phosphoryl transfer. In the crystal structure, the octahedral AlF_4^- moiety was located in the site usually occupied by the γ-phosphate of GTPγS and coordinated axially by the oxygen atoms of GDP (β-oxygen) and an ordered water molecule positioned for in-line nucleophilic attack.

Although AlF_4^- is isoelectronic with the transferring phosphoryl group, the octahedral geometry place demands on the active site architecture evolved to coordinate a trigonal bipyramidal transition state. However, this elegant use of a metal-fluoride moiety mimicking the γ-phosphate geometry of guanosine triphosphate (GTP) opened the possibility to "trap" transition state analog (TSA) complexes of other phosphoryl transfer enzymes, which led to a number of seminal structures that defined the important features needed for catalysis.[5–9]

Aluminum fluoride has since continued to play a leading role in the determination of important high-resolution TSA structures. At the turn of the century, a new metal fluoride species was discovered that self-assembled in the active site and comprised a magnesium cation as the central metal, coordinated axially by donor and acceptor oxygen atoms, together with three fluoride atoms arranged equatorially.[10] With this trigonal bipyramidal geometry, the MgF_3^- moiety thereby represents a closer isoelectronic and isosteric mimic to the transition state of the transferring phosphoryl group than AlF_4^-.

Early metal fluoride screening experiments[11] identified that beryllium trifluoride also possesses enzyme activation and inhibitory properties. However, unlike aluminum fluoride and

Please cite this article in press as: Pellegrini et al., Metal fluorides—multi-functional tools for the study of phosphoryl transfer enzymes, a practical guide, Structure (2024), https://doi.org/10.1016/j.str.2024.07.007

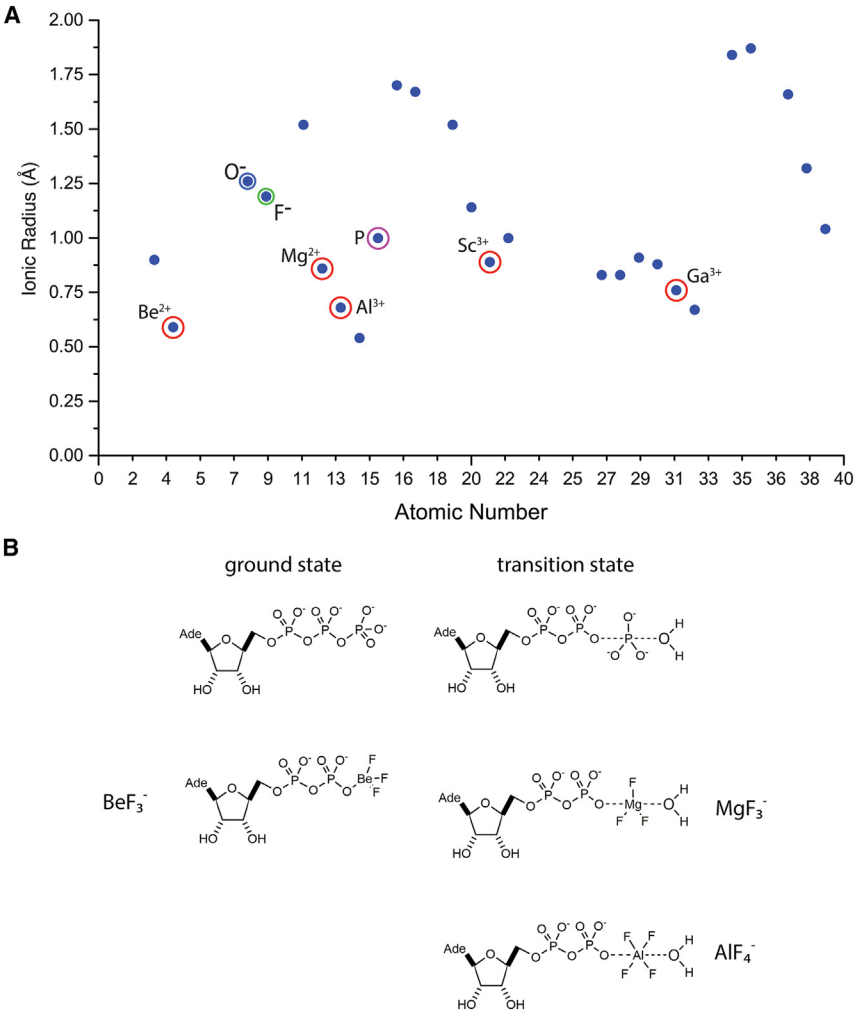

Figure 1. Metal fluoride properties

(A) Ionic radii of selected elements. The ionic radii[17] of elements are plotted in Ångstroms against the atomic number (except for phosphorus where the atomic radius is shown). The relationship between phosphorus and the metals that form phosphoryl analogs with fluoride is shown. The scandium-fluoride bond is the longest observed at 2 Å and may represent the limit for the largest ionic radius tolerated in the active sites of phosphoryl transfer enzymes.

(B) Schematic of metal fluorides compared to the ground state and transition state of the hydrolysis of ATP as an example.

magnesium fluoride, species which can adopt near-transition state geometries, the coordination of beryllium fluoride is strictly tetrahedral in enzyme complexes and thereby is an excellent mimic of a ground state phosphate group. A wide variety of enzyme complexes containing a BeF_3^- species have been described crystallographically.[12–16] A detailed description of all available metal fluoride structures can be found in Jin et al. 2017.[16]

Here, we describe the best protocols to obtain these complexes, their various uses in structural biology and present a cross-soaking strategy that allows ground state complexes to be formed from metal fluoride bound complexes. We also present the structure of a new metal fluoride, scandium tetrafluoride, that places an anomalously scattering element in the active site of phosphoryl transfer enzymes, and compare it with the equivalent AlF_4^- complex.

RESULTS AND DISCUSSION

Comparison of metal fluorides and phosphate groups

The three primary metal fluorides described preeviously provide the perfect tool kit to study phosphoryl transfer enzymes. Fluorine and oxygen have very similar ionic radii[17,18] (Figure 1A), share the same valence orbitals, and have strong propensities to form hydrogen bonds with hydrogen donors, making fluorine an excellent surrogate for oxygen. The three metals are close to phosphorus, either in ionic radius or periodicity, but each has different properties and different electrons available for hybridization, leading to different possible coordination numbers and geometries (Figures 1B and 2A). Together with fluoride, these metals form excellent analogs of phosphoryl groups in the active sites of enzymes.

Principal advantages of the use of metal fluorides

Trap enzymes in stable, functionally relevant conformations

Many enzymes perform catalysis by involving large conformational changes throughout the reaction coordinate, such as the re-structuring of mobile loops, domain-domain closure events, or in the binding of large substrates such as RNA.[6,19–21] Similar changes are observed in structural proteins, such as tubulin and actin.[22,23] These dynamics can make it difficult to either study catalytically relevant conformations and structural intermediates or maintain a sufficiently homogenous population to allow crystallization to occur, or enough particles to be selected to obtain a meaningful 3D reconstruction in cryo-EM. By the formation of very stable complexes, the use of metal fluorides can remove or reduce protein flexibility and fix phosphate-transferring enzymes into an active and immobile state. Such states provide structural homogeneity and therefore excellent starting points for crystallization trials or other studies.[24]

Study of the reaction mechanism; insights into catalysis

In addition to the structural possibilities provided by the use of transition state analogs, the ability to sample a ground-state analog complex by the use of BeF_3^- allows for comparison of structure throughout the various stages in the reaction coordinate. By combining a series of enzyme complexes containing metal fluoride analogs of the ground state and transition state, the interaction of active site residues with surrogates of the

Please cite this article in press as: Pellegrini et al., Metal fluorides—multi-functional tools for the study of phosphoryl transfer enzymes, a practical guide, Structure (2024), https://doi.org/10.1016/j.str.2024.07.007

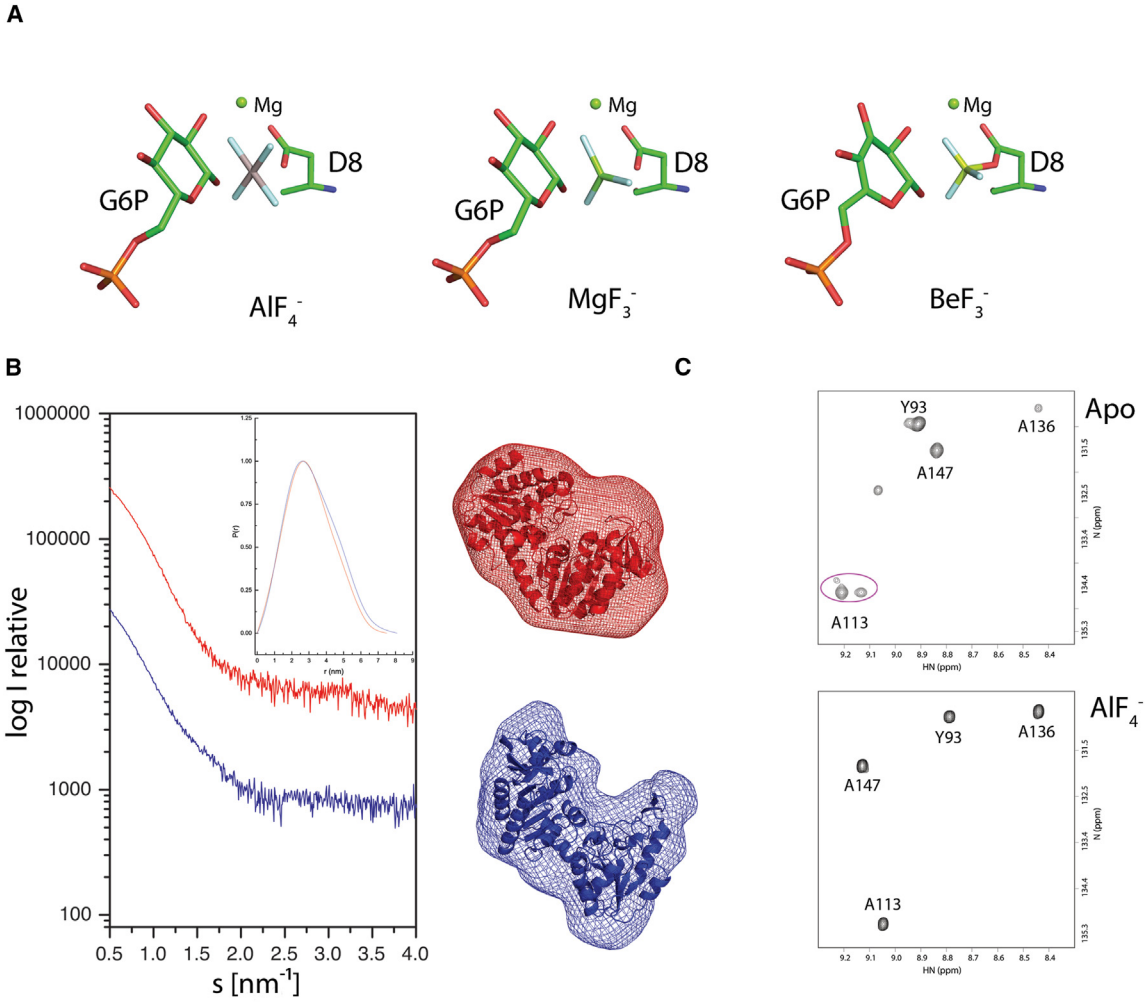

Figure 2. Metal fluorides and their uses

(A) Examples of enzyme-metallofluoride complexes. AlF_4^- (PDB: 2WF6) and MgF_3^- (PDB: 2WF5) are shown in the active site of βPGM where they mimic the transition state of the phosphoryl transfer between glucose-1,6-bisphosphate (G6P) and the catalytic aspartate (D8). BeF_3^- (PDB: 2WF9) is shown in the active site of βPGM where it mimics the phosphoaspartyl intermediate of the catalytic cycle.

(B) Aluminum fluoride traps the active closed state of PGK in solution allowing it to be compared to the *apo*enzyme. Scattering curves, distance distribution functions (inset chart) and *ab initio* shapes determined from SAXS data recorded on *apo* PGK (PDB: 2YAG) and the PGK-3PG-AlF_4^--ADP TSA complex (PDB: 2WZC) and the structures fit to the envelopes. Data from the *apo* protein are shown in *blue* and from the aluminum fluoride complex *red*.

(C) Identical regions of ^1H-^{15}N TROSY spectra recorded on substrate free βPGM and the βPGM-AlF_4^--G6P TSA complexes using standard NMR conditions. For substrate free βPGM, slow exchange dynamics arising from *cis-trans* proline isomerization result in the presence of multiple peaks for selected residues[61] (magenta ellipse). The cap and core domains of substrate-free βPGM are arranged such that the active site is open (PDB: 2WHE). For the βPGM-AlF_4^- -G6P TSA complex, single peaks indicate that these slow dynamics present in the open state have been arrested, confirming the ability of AlF_4^- to act as molecular glue stabilizing the fully closed enzyme (PDB: 2WF6).

oxygen atoms of the phosphoryl group may be visualized for the complete phosphoryl transfer reaction.

Convenience

Finally, metal fluoride complexes are both simple and inexpensive to prepare and have potential application in any enzyme system that involves phosphoryl transfer or phosphate binding. As they are intrinsically unreactive species, their use avoids the necessity of non-hydrolyzable substrate analogs that often have lower binding affinities than the cognate substrate and may introduce structural distortions. The presence of electron-rich metal ions and fluorine nuclei in the active site also opens specific avenues for X-ray diffraction and NMR analyses.

Choosing the right tool for the job

AlF_4^-

The most commonly used metal fluoride ion, aluminum tetrafluoride, has octahedral geometry (Figures 1B and 2A) and forms the most stable complexes with proteins and substrates. Its charge density is the highest and, as it is also present as a free species in solution,[25] it does not require a fully formed active site in which to assemble. This makes it the first choice as "molecular glue" to trap the active state of an enzyme in solution, despite having a planar geometry (octahedral) different from that of the native transition state (trigonal bipyramidal). We have shown that AlF_4^- stabilizes these conformations in solution

Please cite this article in press as: Pellegrini et al., Metal fluorides—multi-functional tools for the study of phosphoryl transfer enzymes, a practical guide, Structure (2024), https://doi.org/10.1016/j.str.2024.07.007

before crystallization using both SAXS and NMR (Figures 2B and 2C) thereby trapping the conformation for further study. These solution techniques demonstrate that the substrate-bound closed conformations of both PGK and PGM are trapped prior to further experiments. AlF_4^- stabilizes these states by strongly coordinating substrates and active site residues. Many structures in the PDB contain the trigonal bipyramidal species AlF_3. The difference between the two species was originally thought to be induced by pH change.[26] However, as aluminum ions precipitate as a hydroxide at high pH,[25] it is likely that these structures actually contain MgF_3^{-10}. While AlF_3 is observed in solution, it is most likely octahedrally coordinated with a third water molecule, similar to the species observed in the PGK mutant K219A.[19]

MgF_3^-

Magnesium trifluoride ions also form transition state analog complexes, but these have different properties from those formed by AlF_4^-. First, as well as being isoelectronic with the transferring phosphoryl group, MgF_3^- ions are isosteric, adopting a trigonal bipyramidal geometry that mimics the transition state moiety (Figures 1B and 2A). The combination of these properties makes trifluoromagnesate ions much closer analogs of the transition state of phosphoryl transfer. However, the formation constant of MgF_3^- ions in free solution is extremely low,[27] which demands that the ion can only assemble directly in the active sites of enzymes.[25] As a result, the overall affinity of the MgF_3^- ion is frequently found to be much lower than that of AlF_4^-. However, due to its closer match to the transition state, MgF_3^- complexes are preferable for detailed analysis of catalytic mechanisms, compared to the ones formed by AlF_4^-.

While the majority of structures containing trifluoromagnesate ions demonstrate trigonal bipyramidal geometry, there are a small number of examples where alternative geometries are observed. An octahedrally coordinated $MgF_3(H_2O)^-$ has been characterized and shed light on the catalytic mechanisms of some phosphoryl transfer enzymes with more flexible active sites.[28,29] Additionally, the SERCA Ca^{2+} ATPase has been crystallized with a putative tetrahedrally coordinated MgF_4^{2-} species.[30]

BeF_3^-

Beryllium trifluoride ions have obligate tetrahedral geometry and therefore form analogs that are isosteric and isoelectronic with the ground state of phosphoryl transfer (Figures 1B and 2A). The crystal structures of BeF_3^- and MgF_3^- complexes place the fluoride ions in the locations of both ground and transition states and therefore provide the best starting points for modeling studies of the enzyme active site. BeF_3^- also has a role for proteins other than phosphoryl transfer enzymes, as it has been successfully used to mimic the phosphate moiety bound at phosphorylation sites, leading to structural and functional properties which mimic those of the phosphorylated protein.[13,31] This behavior is particularly useful as homogeneous populations of phosphoproteins can be difficult to prepare. Additionally, as beryllium has higher solubility than aluminum,[32] high concentrations of beryllium fluoride can be used to drive low-affinity active states, such as with G proteins in the absence of a GAP.[33]

Forming metal fluoride complexes

The model systems β-phosphoglucomutase (βPGM) and human phosphoglycerate kinase (PGK) catalyze different phosphoryl transfer reactions, and in combination with metal fluoride moieties, both ground state and transition state analog complexes have been investigated, using a variety of structural techniques, to define several aspects of catalysis.[19,24,25,31,34–39] Here, we use these model systems to illustrate how to form the complexes and how to best exploit their various properties.

The great advantage of metal fluoride TSA and ground state analog (GSA) complexes is that all components are present in solution and readily self-assemble in the active site forming stable enzyme complexes that are relevant to the catalytic cycle. The inorganic metal fluoride salts (AlF_3 and MgF_2) are too insoluble to use and therefore, the fluoride anion and metal cation components must be added from separate stock solutions. Caution should be employed when preparing these solutions as the reaction is exothermic; the use of a fume hood is recommended. Both ammonium fluoride and sodium fluoride are suitable as the source of fluoride and are readily soluble in water. No difference between the salts is observed in the formation of the metal fluoride protein complex but a difference may be apparent in crystallization trials where the counter ion can have an effect on crystal packing. Metal chlorides, such as $AlCl_3$, $MgCl_2$, $BeCl_2$, $GaCl_3$, and $ScCl_3$ can be easily dissolved in water at high concentration (0.5 M) and the solutions conserved at −20°C. One of the critical aspects in preparing metal fluoride enzyme complexes is the pH of the resulting solution. In particular, solutions of $AlCl_3$, $BeCl_2$, $GaCl_3$, and $ScCl_3$ are highly acidic (pH ∼2), and the addition of even small volumes of a solution at this pH value to a protein sample will cause precipitation. As the tolerance of protein precipitation within samples is quite different for crystallization and NMR studies, the preparation process of the metal chloride stock solutions and the protein samples is optimized in different ways. Of particular importance are the pH adjustment of the stock solutions and the sequence of component addition.

In transition state analog complexes, the axial ligands of the metal fluoride ions correspond to the phosphate donor and acceptor oxygen atoms of the transferring phosphate group. Therefore, for the formation of the complex the native substrate(s)—lacking the phosphate which the metal fluoride mimics—must also be present in solution. For example, βPGM requires glucose-6-phosphate (G6P) or β-glucose-1-phosphate (Figure 2A), phosphoserine phosphatase requires serine or H_2O, and phosphoglycerate kinase requires both ADP and 3-phosphoglycerate (3PG). In most cases, such metal fluoride complexes require the presence of the product or cofactor of the enzymatic reaction in stoichiometric excess.

BeF_3^- ground state complexes have been shown to form either when both phosphate acceptor and donor molecules are present or when only one is present. For example, BeF_3^- complexes of βPGM can form in the presence (PDB: 2WF8 and 2WF9) or absence (PDB: 2WFA) of the phosphate acceptor molecule G6P.[31] In both cases, the BeF_3^- ion is found to be axially coordinated by the catalytic aspartate residue (D8) that acts as the nucleophile in the active site of βPGM (Figure 2A). Indeed in all BeF_3^- complexes of phosphoryl transfer enzymes studied so far, the BeF_3^- ion is found coordinated to the most acidic of the two available acceptor/donor groups.[16]

Sample preparation for crystallization, SAXS and cryo-EM

In order to increase the pH values of the metal chloride stock solutions, they should be prepared in 100 mM unbuffered Tris base.

Please cite this article in press as: Pellegrini et al., Metal fluorides—multi-functional tools for the study of phosphoryl transfer enzymes, a practical guide, Structure (2024), https://doi.org/10.1016/j.str.2024.07.007

In the case where an AlF_4^- complex is desired, the protein buffer must be maintained below pH 7.5 to guarantee the aluminum cation solubility. Titration experiments monitored using ^{19}F NMR spectroscopy have shown that AlF_4^- and $AlF_3(OH)^-$ species in solution are pH dependent and above pH 8 aluminum cations are precipitated from solution as insoluble aluminum hydroxide.[25,40] Under these aluminum limited conditions, only trigonal bipyramidal MgF_3^- TSA complexes can be obtained, given sufficient magnesium ions in the buffer.[16,25] Therefore, the optimized sequence of component addition is to add fluoride to the protein buffer first, then the metal chloride stock, thereby allowing the formation of metal fluoride solution species first. Following pH re-adjustment, the protein stock solution is added to the final protein buffer together with the substrate required for the TSA or GSA complexes. In this manner, the chances of forming stable metal fluoride complexes while maintaining solubility of both protein and metal cations are increased. Typical concentrations for the components are 10–40 mM fluoride ions, 5–20 mM magnesium ions, 1–5 mM aluminum ions, 1–10 mM beryllium ions, 10 mM scandium ions, and 10 mM gallium ions. These concentrations need to be reduced for cryo-EM studies as high concentrations can increase background noise when the particle size of the sample is small (<100 kDa). In these cases, reducing the concentrations to 250 μM fluoride ions and 25 μM metal ions improves signal to noise significantly while maintaining the complex.[41]

Sample preparation for NMR studies

The protein concentrations used in NMR (and crystallization) experiments are usually relatively high (0.5–1 mM) compared to biochemical assays. Therefore, in order to avoid unnecessary dilution of the protein component, the ingredients are added directly to the buffered protein stock at neutral pH containing an appropriate concentration of $MgCl_2$ as the source of the metal catalytic cofactor and 1–2 mM NaN_3 as a preservative. The metal chloride stock solution ($AlCl_3$, $BeCl_2$, $ScCl_3$, or $GaCl_3$) and fluoride stock solution (NH_4F or NaF) are added first to inhibit any trace of residual enzyme activity, followed by the substrate. Any unwanted protein precipitate generated during the sample preparation procedure can be removed effectively by centrifugation prior to transferring the sample into the NMR tube. Typical concentrations for the components are 10–40 mM fluoride ions, 5–20 mM magnesium ions, 1–3 mM aluminum ions, 1–5 mM beryllium ions, 10 mM scandium ions, and 10 mM gallium ions. However, the fluoride concentrations used here can leach aluminum ions from glass NMR tubes (Wilmad-LabGlass, NJ), particularly if in contact for extended periods (>2–3 days), and so for experiments involving MgF_3^- TSA complexes, the sample should be supplemented with 1–2 mM deferoxamine, which is a potent chelator of aluminum cations. For ^{19}F NMR experiments recorded in 100% H_2O buffer, the deuterium NMR lock is provided by external 100% D_2O buffer present in a sealed glass capillary tube inserted in the conventional NMR tube.

X-ray crystallography methods

Cross-soaking

The ability to trap proteins with a TSA can help in the understanding of the reaction mechanism but reveals little information concerning the binding of the ground states in the reaction coordinate or of the binding of other ligands or inhibitors. The glycolytic enzyme PGK has been studied for many years as a classical hinge-bending enzyme, but all crystal structures obtained were in open or semi-open conformations.[42,43] Using metal fluorides, we were able to obtain the first fully closed structures, demonstrating how the active site arranged around the transition state.[19] However, attempts to crystallize this closed conformation of PGK in the presence of ADP, ATP analogs (AMP-PNP and AMP-PCP), or BeF_3^- failed, as these complexes cannot maintain the closed state, presenting a flexible complex for crystallization.[24] In order to obtain the closed conformation in complex with GSAs, we tried a practice known as cross-soaking, which has been shown to be effective with peptides and other ligands.[44–47] We found that for PGK, MgF_3^-, and AlF_4^- can be used to trap the closed conformation for crystallization and subsequently be removed and a new ligand soaked in while maintaining the closed conformation. Crystals of the MgF_3^-, ADP, 3PG quaternary complex (PGK-3PG-MgF_3^--ADP TSA complex PDB: 2WZB) were soaked in buffers that matched the mother liquor but were devoid of fluoride ions. Soaking times were varied and datasets collected on crystals harvested at 10 min intervals (see Table 1 for details of data reduction and refinement and STAR Methods for detailed crystallographic methods). The optimal time for complete removal of the metal fluoride was found to be 30 min (this will of course vary, depending on the system being studied, the solute accessibility of the active site and crystal packing) and the absence of the TSA was confirmed by analysis of the difference Fourier maps (Figure 3A) resulting in the PGK-3PG-ADP structure (PDB: 2X13). We then attempted to soak in the GSA AMP-PCP and found that a further 30 min was then required to allow the analog to enter the active site and displace the remaining ADP (Figure 3B). These cross-soaking experiments enabled the structure of PGK to be obtained in its closed state with the phosphonate analog AMP-PCP bound in its active site, though this was only successful in the case of the K219A variant (PGK(K219A)-3PG-AMPPCP GSA complex PDB: 2X14). This may be either because the hydrogen bond network cannot accommodate the bridging methylene of AMP-PCP which could prevent binding or that the methylene bond is too long for the highly constrained active site where it could clash with the side chain of K219 in the wild type.[48] A structure of wild type PGK bound to AMP-PCP exists (PDB: 2XE8), however it is in the open conformation and there are no constraints around the γ-phosphonate as it is solvent exposed.[24] For the PGK-3PG-BeF_3^--ADP GSA complex (PDB 4AXX) the aforementioned procedure was followed except that after removal of the metal fluoride the crystal was then placed into the mother liquor containing 10 mM ammonium fluoride and 20 mM $BeCl_2$ for 30 min, to introduce the ground state analog (Figure 3C). The high concentration of beryllium was needed to compete with any formation of MgF_3^- from the catalytic magnesium present.

As metal fluorides are ionic species, this property allows the ions to diffuse out from the active site when the crystals are presented with a solution where they are absent. The lower intrinsic stability of the ionic species MgF_3^- means that it can diffuse out of the active site when the crystals are placed in a buffer lacking fluoride ions, but we have successfully removed both aluminum and magnesium species. Crystal packing maintains the protein

Please cite this article in press as: Pellegrini et al., Metal fluorides—multi-functional tools for the study of phosphoryl transfer enzymes, a practical guide, Structure (2024), https://doi.org/10.1016/j.str.2024.07.007

Table 1. Data collection and refinement statistics for PGK closed conformation cross soaks

Structure	PGK-3PG-ADP	PGK (K219A)-3PG-AMPPCP	PGK-3PG-BeF_3^--ADP
PDB code	2X13	2X14	4AXX
Space group	$P2_12_12_1$	$P2_12_12_1$	$P2_12_12_1$
Wavelength	0.933 Å	0.933 Å	0.933 Å
Unit cell dimensions (Å) a, b, c	38.9, 91.4, 108.5	39.4, 91.5, 108.4	38.8, 90.8, 108.5
Resolution range (Å)	20–1.74 (1.83–1.74)	20–1.90 (2.0–1.90)	20–1.74 (1.83-1.74)
Number of unique reflections	40002	27244	34680
Multiplicity[a]	3.7 (3.5)	3.0 (2.9)	3.5 (3.2)
Completeness[a] (%)	98.4 (97.0)	86.1 (70.3)	86.9 (89.9)
R_{merge}[a,b]	0.08 (0.26)	0.09 (0.27)	0.07 (0.57)
$\langle I/\sigma(I)\rangle$[a]	9.1 (3.0)	8.1 (3.2)	11.9 (2.3)
Wilson B factor	18.7 $Å^2$	18.8 $Å^2$	19.7 $Å^2$
Average B factor: ($Å^2$)	22.2	22.1	22.5
Protein	22.8	22.8	21.7
Ligand	14.2	14.7	23.9
Water	22.6	22.5	27.5
Water molecules	279	218	423
R factor[c] (%)	18.5	18.7	17.0
Free R factor[d] (%)	21.8	22.8	20.7
RMS deviations:			
Bonds (Å)	0.011	0.014	0.012
Angles (°)	1.41	1.47	1.54

The PGK-3PG-ADP complex (2X13) was obtained by soaking crystal of the PGK-3PG-MgF_3^--ADP complex (2WZC) in the absence of fluoride ions. The PGK (K219A)-3PG-AMPPCP complex (2X14) was obtained by soaking crystals of the PGK(K219A)-3PG-AlF_3^--ADP (2WZD) complex in the absence of aluminum and fluoride ions and in the presence of AMP-PCP. The PGK-3PG-BeF_3^--ADP complex (4AXX) was obtained by soaking crystal of the PGK-3PG-MgF_3^--ADP complex (2WZC) with 20 mM $BeCl_2$ in addition to magnesium and fluoride ions.

[a]Statistics for the highest resolution bin (1.83–1.74 - ADP; 2.0–1.90 – AMP-PCP; 1.83–1.74 BeF) are shown in parenthesis.

[b]$R_{merge} = \sum_h \sum_i |I(h) - I(h)_i| / \sum_h \sum_i I(h)_i$, where I(h) is the mean weighted intensity after rejection of outliers.

[c]$R = \sum hkl ||F_{obs}| - K|F_{calc}|| / \sum hkl |F_{obs}|$, where F_{obs} and F_{calc} are the observed and calculated structure factor amplitudes.

[d]$R_{free} = \sum hkl \subset T ||F_{obs}| - K|F_{calc}|| / \sum hkl \subset T |F_{obs}|$, where F_{obs} and F_{calc} are the observed and calculated structure factor amplitudes and T is the test set of data omitted from refinement (5% in this case).

conformation initially stabilized by the metal fluoride and allows alternative ligands to be inserted;in this way, the active conformation in the presence of an ATP analog (PDB 2X14) and the BeF_3^- complex with 3PG, mimicking the 1,3-bisphosphoglycerate (1,3BPG) complex (PDB: 4AXX), were determined (see Table 1 and STAR Methods for detailed crystallographic methods) allowing a complete structural description of the reaction to be obtained (Figure 3D).

Potential phasing applications of metal fluoride complexes

A number of derivatized nucleotide compounds have been developed that allow the insertion of a heavy atom into the active site of a nucleotide binding protein. These nucleotides contain a halogen[47,49] or a selenium atom[50] that serve as anomalous scattering centers, either to locate the nucleotide binding site in low resolution structures[51] or to be used in MAD or SAD phasing experiments.[52] These compounds are very useful; however, they are only effective for proteins that bind nucleotides and can be costly to synthesize. Given that magnesium, aluminum and beryllium all form protein metal fluoride complexes, the possibility of making complexes with metals that have a K-absorption edge within the energy range available at synchrotron radiation sources can be investigated as a potential source of new phasing compounds. It has been reported that myosin can be inhibited by scandium and gallium fluorides in addition to aluminum, magnesium, and beryllium[53] and this was used as a starting point to screen the presence of fluoride complexes with metals having a K-absorption edge relevant to protein crystallography. Using βPGM as a model, a series of 10 metals (Ca, Sc, Co, Ni, Cu, Zn, Ga, Ge, Sr, and Y) were screened using ^{19}F-NMR and crystallography for the formation of protein-bound metal fluoride complexes, with only scandium and gallium tetrafluoride complexes observed (Figure 4A). The structure of the scandium tetrafluoride complex of βPGM (βPGM-ScF_4^--G6P TSA complex (PDB: 3ZI4)) was determined at 1.3 Å and compared to the aluminum complex (βPGM-AlF_4^--G6P TSA complex (PDB: 2WF6)) determined at a similar resolution[34]; see Table 2 for details of data reduction and refinement (see STAR Methods for detailed ^{19}F-NMR and crystallographic methods).

As expected, scandium (III) forms an octahedrally coordinated tetrafluoride moiety between the catalytic aspartate residue (D8) and the 1-hydroxyl group of G6P in the βPGM active site resulting in a near-transition state complex (Figure 4B). This novel ScF_4^- species binds in a similar manner to its AlF_4^- counterpart but has longer metal fluoride bonds, 2.0 Å vs. 1.8 Å, respectively (Figure S1) and axial oxygen distances at 2.0 Å and 2.2 Å. The scandium atom was positively identified as occupying the position of the central metal by the collection of a dataset at an energy of 7 keV (λ = 1.77 Å). At this wavelength the anomalous scattering length from scandium is 1.95 electrons (against 0.56 electrons for phosphorus and 0.72 electrons for sulfur). Inspection of the anomalous difference Fourier maps revealed a peak of 15.4σ at the position of the central metal (Figure 4B), thereby confirming for the first time the atomic identity of the central metal in a metallofluoride. Therefore, ScF_4^- species can be used to trap enzymes in near-transition state conformations, additionally identifying the location of active sites and facilitating SAD phasing protocols where it would contribute considerably to the anomalous signals from native sulfur and/or phosphorus atoms. Enzyme TSA complexes involving GaF_4^- species would be extremely useful for MAD phasing experiments as its K-absorption edge is at 10.37 keV (λ = 1.20 Å) within the energy range available at macromolecular crystallography beamlines. We obtained crystals of the ScF_4^- complex but not of the corresponding gallium complex, though the latter was detectable

Please cite this article in press as: Pellegrini et al., Metal fluorides—multi-functional tools for the study of phosphoryl transfer enzymes, a practical guide, Structure (2024), https://doi.org/10.1016/j.str.2024.07.007

CellPress
OPEN ACCESS

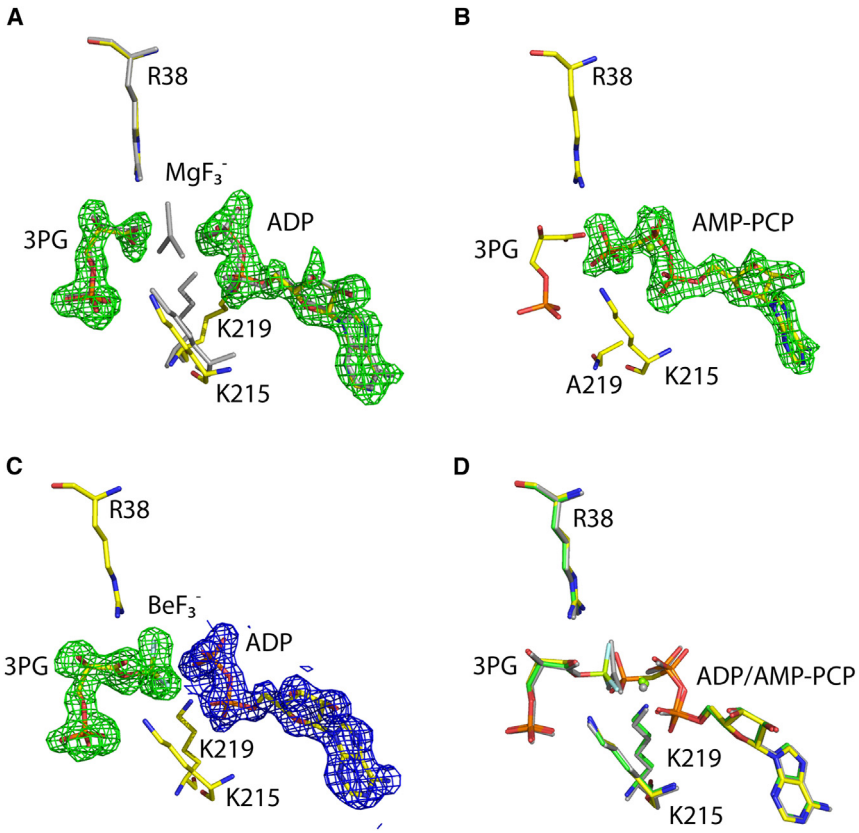

Figure 3. Cross soaking to obtain ground state complexes in the closed conformation of PGK

(A) Structure of the PGK-3PG-ADP complex (2X13) carbon atoms yellow. Initially crystals of PGK-3PG-MgF_3^--ADP TSA complex (2WZC) were soaked in a buffer lacking fluoride ions and the structure determined. The difference Fourier demonstrates the complete removal of the transition state analog and the movement of a catalytic lysine (K219) also confirms the removal (the PGK-3PG-MgF_3^--3PG TSA complex (2WZC) is shown in gray for reference).

(B) Structure of the PGK(K219A)-3PG-AMPPCP complex (2X14) carbon atoms yellow. Once the transition state analog is removed new ligands can be soaked in – here, AMP-PCP replaces ADP showing the ATP ground state.

(C) The structure of the PGK-3PG-BeF_3^--ADP complex (4AXX), carbon atoms yellow. When beryllium ions are added, the map shows the ground state analog coordinated to 3PG mimicking the 1,3-BPG complex.

(D) When combined with the transition state analog complex, a complete description of catalysis is obtained (AMP-PCP carbon atoms yellow, 3PG-BeF_3^- carbon atoms green and PGK-3PG-MgF_3^--3PG TSA complex is shown in gray). Difference maps (green) are shown contoured at 3σ and $2mF_o-F_c$ maps (blue) are shown contoured at 1.5σ. The structures shown are the PGK-3PG-MgF_3^--ADP TSA complex (2WZC), the PGK(K219A)-3PG-AMPPCP complex (2X14) and the PGK-3PG-BeF_3^--ADP complex (4AXX).

in solution (Figure 4A), which may be due to the requirement of a low pH being incompatible with the crystallization conditions for βPGM, as Ga^{3+} ions, but not Sc^{3+} ions, precipitate as $Ga(OH)_3$ at pH values above 6.0.

The metals that have been shown to form enzyme-metallofluoride complexes all fall within a close ionic radius and/or periodic range[17,18] (Figure 1A). The ability of the metal fluoride moieties to self-assemble in the active sites of phosphoryl transfer enzymes is probably dependent on the electronic configuration but also the radius of the ion. The metal-fluoride bonds that have been characterized vary from 1.6 Å in BeF_3^-,[31] 1.8 Å in AlF_4^-, 1.9 Å in MgF_3^- [10,34] and 2.0 Å in ScF_4^-, whereas the phosphoryl oxygen bond varies between 1.5 Å and 1.7 Å. Therefore, the ionic radius of scandium (0.89 Å)[17,18] probably represents the maximum for a metal fluoride that is readily tolerated in an enzyme active site.

^{19}F-NMR

^{19}F-NMR properties

^{19}F NMR studies of protein complexes involving fluorinated compounds or metal fluoride moieties are attractive as the ^{19}F nucleus occurs at 100% natural abundance, is spin ½ with high sensitivity (83% of ^{1}H) and has a large chemical shift range (100-fold larger than ^{1}H). The resulting spectra are also relatively simple to interpret since they are free from background signals.[54,55] Solution ^{19}F NMR was first applied to protein systems in the late 1960s[56] and one of the primary advantages of this technique is to report on the structures of known protein systems in their native solution environment. Since the ^{19}F spectra for metal fluoride complexes show only few and usually well-resolved peaks, in contrast to ^{1}H, ^{13}C, and ^{15}N spectra, the molecular weight restrictions that impact NMR approaches using multidimensional strategies are alleviated such that systems as large as 200 kDa can be studied. The ^{19}F chemical shift is extremely sensitive to changes in local electrostatics and alterations in van der Waals contacts. Hence, for enzyme-metallofluoride TSA and GSA complexes, ^{19}F NMR spectroscopy offers an extremely sensitive approach with which to probe atomic environments in the vicinity of the phosphate oxygen atoms in catalytically relevant active site geometries.[16] ^{19}F chemical shift values, solvent induced isotope shifts (SIIS) observed on the ^{19}F resonances, linewidth measurements, cross-hydrogen bond F—HN scalar $^{1}J_{HF}$ and $^{2}J_{NF}$ couplings and driven-1H and transient-1H nuclear Overhauser effects (NOEs) (see the following text for details of each) all report on interatomic proximities in the solution state[25,34] which can be correlated with high-resolution crystal structures.

^{19}F chemical shifts

^{19}F resonances display a very large chemical shift range (~1,000 ppm) and are predictable with good precision from quantum calculations of electronic distributions.[57] However, the chemical shift range observed for ^{19}F resonances in enzyme-metallofluoride complexes is lower and in general they locate between −125 ppm and −195 ppm, when using $CFCl_3$ resonating at 0.0 ppm as the IUPAC referencing standard. Since the ^{19}F chemical shift is sensitive to the van der

Please cite this article in press as: Pellegrini et al., Metal fluorides—multi-functional tools for the study of phosphoryl transfer enzymes, a practical guide, Structure (2024), https://doi.org/10.1016/j.str.2024.07.007

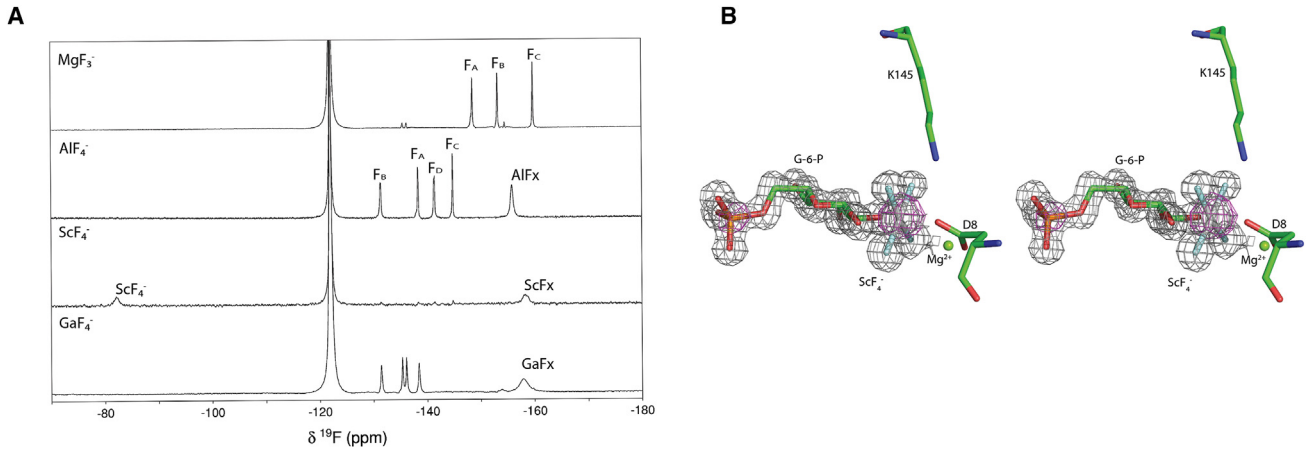

Figure 4. New metal fluorides

(A) ^{19}F NMR spectra for βPGM-G6P TSA complexes with MgF_3^-, AlF_4^-, ScF_4^-, and GaF_4^- (top to bottom) occupying the site of the transferring phosphoryl group. The sharp GaF_4^- complex resonances appear at roughly similar frequencies to those of the previously reported AlF_4^- complex, with chemical shifts of −131.4, −135.3, −136.1 and −138.4 ppm. In the ScF_4^- complex, a single broad protein-dependent peak appears at −82.2 ppm, suggesting rotational averaging of the ^{19}F environments in solution. In all cases the free F^- ion resonance appears at −122.0 ppm, and for the AlF_4^-, ScF_4^- and GaF_4^- complex spectra, the broad peaks upfield of −150 ppm are the result of free metal fluoride species in solution. Both Sc and Ga have K edges accessible to, or near, the energies available at synchrotron beamlines.

(B) Stereo image of the active site of the βPGM-ScF_4^--G6P complex structure (PDB 3ZI4). The $2mF_o-F_c$ map from native data collected to 1.3 Å is shown as a gray mesh contoured at 1.5σ and the anomalous difference Fourier calculated from data collected at 7 keV is shown as a magenta mesh contoured at 5σ. The scandium atom is clearly identified by a 15.4σ peak in the anomalous difference maps; the corresponding peak for the phosphorus atom is 8.5σ.

Waals environment as well as local electrostatic fields, the relative chemical shift positions within this range are highly sensitive to differential proton densities. This sensitivity is illustrated, for example, by the significant upfield chemical shift observed for the most upfield peak (Fc) between the βPGM-MgF_3^--G6P and βPGM-MgF_3^-2-deoxy-G6P TSA complexes (compare spectra (a) and (c) in Figure 5A).[35] Here, the removal of a contributing hydrogen bond between the sugar phosphate and the metal-fluoride results in the fluorine nucleus being significantly more shielded (Figure 5E).

Solvent induced isotope shifts

Solvent induced isotope shifts (SIIS), defined as SIIS = $\delta X(H_2O) - \delta X(D_2O)$ where $\delta X(H_2O)$ is the chemical shift of nucleus X in 100% H_2O buffer and $\delta X(D_2O)$ is the chemical shift in 100% D_2O buffer,[58] are widely used to examine the environment of fluoride ions in protein complexes.[16] The substantial magnitudes of SIIS for enzyme-metallofluoride complexes is illustrated by comparing spectra (a) with (b), and (c) with (d) in Figure 5A. For free fluoride in solution, the SIIS observed is close to 3.0 ppm at 298 K, which represents a maximal effect and arises from through-space transmission of the electric field differences between F—H and F—D solvation. The extent of the isotope shift in enzyme-metallofluoride complexes depends on the number of the substitutable hydrogen atoms in the vicinity of the fluorine nuclei and also on the distance and angle of the coordinating hydrogen bonds.[59,60] For F···H–N and F···H–O hydrogen bonds between the metal fluoride moiety and the protein, the magnitude of the SIIS reflects the local proton densities around each fluorine nucleus.[34,35] A high proton density generates a deshielded fluorine nucleus resulting in large SIIS values and downfield chemical shifts approaching that of highly solvated free fluoride (Figures 5B and 5E). Conversely, the most upfield fluorine resonances always have the smallest SIIS values and line widths and are coordinated primarily by the essential catalytic magnesium cation with a concomitant low density of hydrogen bond donors. Partial deuteration can also be used to help the assignment of individual ^{19}F resonances according to their coordination by Lys or Arg sidechains and to determine the contributions to overall SIIS values by individual hydrogen atoms.[16]

J coupling

The presence of well-defined and long-lived hydrogen bonds involving protein backbone amide groups and fluorine atoms in the active site has enabled the measurement of cross-hydrogen bond $^1J_{HF}$ and $^2J_{NF}$ scalar coupling constants in ^1H,^{15}N-HSQC experiments recorded without ^{19}F decoupling.[34,35] Here, the enzyme-metallofluoride complexes need to be prepared with ^{15}N-labeled protein so that the previously assigned backbone HN peaks are split horizontally by the one-bond ^1H-^{19}F coupling and vertically by the two-bond ^{15}N-^{19}F coupling for amide groups participating in hydrogen bonds to fluorine. Application of ^{19}F decoupling in both the ^{15}N and ^1H dimensions of the ^1H,^{15}N-HSQC pulse program results in a collapse of the scalar coupled peaks to an averaged position, confirming the involvement of fluorine in the effect (Figure 5D). The magnitudes of both coupling constants correlate closely with interatomic distances derived from high resolution crystal structures, providing independent validation of the similarity of enzyme-metallofluoride complexes in the solution and solid state (Figure 5C).

NOEs

The close proximity and long residence times of fluorine atoms in near-transition state and ground state analog complexes allows the specific assignment of fluorine nuclei to their atomic

Please cite this article in press as: Pellegrini et al., Metal fluorides—multi-functional tools for the study of phosphoryl transfer enzymes, a practical guide, Structure (2024), https://doi.org/10.1016/j.str.2024.07.007

Table 2. Data collection and refinement statistics for βPGM structures

Structure	βPGM-ScF_4^--G6P native	βPGM-ScF_4^--G6P long wavelength
PDB code	3ZI4	
Space group	$P2_12_12_1$	$P2_12_12_1$
Wavelength (Å)	0.933	1.77
Unit cell dimensions (Å) a, b, c	37.2, 54.2, 104.6	37.2, 54.2, 104.5
Resolution range (Å)	20–1.33 (1.4–1.33)	20–1.95 (2.06–1.95)
Number of unique reflections	46171	15433
Multiplicity[a]	3.4 (3.0)	12.4 (12.5)
Completeness[a] (%)	94.0 (76.6)	96.3 (92.8)
R_{merge}[a,b]	0.05 (0.45)	0.10 (0.21)
$<I/\sigma(I)>$ [a]	18.7 (2.4)	19.1 (10.8)
Wilson B factor (Å^2)	10.7	14.6
Average B factor: (Å^2)	14.7	
Protein	11.9	
Ligand	14.6	
Water	25.1	
Water molecules	422	
R factor[c]	13.0	
Free R factor[d]	17.4	
RMS deviations:		
Bonds (Å)	0.01	
Angles (°)	1.67	

[a]Statistics for the highest resolution bin (βPGM-ScF_4^--G6P native: 1.4–1.33 Å and βPGM- ScF_4^--G6P long wavelength: 2.06–1.95 Å) are shown in parenthesis.
[b]$R_{merge} = \sum_h \sum_i |I(h) - I(h)_i| / \sum_h \sum_i I(h)_i$, where I(h) is the mean weighted intensity after rejection of outliers.
[c]$R = \sum hkl ||F_{obs}| - K|F_{calc}|| / \sum hkl |F_{obs}|$, where F_{obs} and F_{calc} are the observed and calculated structure factor amplitudes.
[d]$R_{free} = \sum hkl \subset T ||F_{obs}| - K|F_{calc}|| / \sum hkl \subset T |F_{obs}|$, where F_{obs} and F_{calc} are the observed and calculated structure factor amplitudes and T is the test set of data omitted from refinement (5% in this case).

positions as defined in high resolution crystal structures. A driven nuclear Overhauser effect 2D ^{1}H,^{15}N-HSQC difference experiment results in different NOE profiles to nearby backbone amide groups, following selective irradiation of each of the fluorine resonances.[25,31,36] A transient 2D ^{1}H,^{19}F heteronuclear NOE experiment (HOESY) gives direct correlations between proximate ^{1}H and ^{19}F groups.[31] Both NOE experiments require a residue specific backbone assignment for complete interpretation of the data.

Dynamics

Generally for MgF_3^- and BeF_3^- enzyme-metallofluoride complexes, the fluoride ions exchange considerably more slowly between their individual binding sites than the differences in chemical shift (in Hz) associated with these individual sites, i.e., the resonances of the metal fluoride moiety are in the slow exchange regime on the NMR timescale. This behavior gives rise to discrete well resolved peaks in ^{19}F spectra representative of each individual site. Occasionally, particularly for AlF_4^- enzyme-metallofluoride complexes involving nucleotides and for the βPGM-ScF_4^--G6P TSA complex reported here (Figure 4A), the fluoride ions exchange between individual sites more quickly, even though preferred sites are sufficiently stable to be identifiable in the corresponding crystal structures. A large increase in exchange rate leads to the observation of a single peak for the metal fluoride moiety in ^{19}F spectra representative of the average chemical shift of the individual sites, i.e., each fluoride ion visits all the individual binding sites faster than the ^{19}F NMR signal is resolved, termed the fast exchange regime on the NMR timescale. Elevated exchange rates most likely occur through a rotation of the metal fluoride moiety while still bound in the enzyme active site, which is consistent with active site architecture that has a relatively low barrier to the rotation of the equatorial groups within the non-native octahedral geometry. It remains to be established whether such enhanced rotation is related to faster dissociation and reassociation of the groups that coordinate the metal fluoride axially. However, rotational averaging of ^{19}F NMR signals is not widely observed for all octahedral metal fluoride complexes, for example the βPGM-AlF_4^--G6P and βPGM-GaF_4^--G6P TSA complexes each show four discrete well resolved peaks (Figure 4A).

Conclusions

Here, we hope to have provided a useful manual on the preparation and use of metal fluorides for the study of proteins involved in phosphoryl transfer. Each metal fluoride has its own advantages and together they form a versatile tool kit. In addition to being excellent mimics of both the ground state and transition state of phosphoryl transfer they can be used to trap the active conformation of proteins and complexes and form a starting point for further experiments. In our hands, they have enabled us to describe the fully closed transition state analog (TSA) complex of PGK[19] by X-ray crystallography and NMR and determine the first MAP2K-MAP kinase complex by cryoEM.[41] We have also shown that these complexes can be used as a spring board to ground state complexes by using cross-soaking and, by screening further metals, identified gallium and scandium fluoride complexes as new tools to study phosphoryl transfer enzymes. So far, our results have identified no exception of analog formation for wild-type proteins that catalyze phosphoryl transfer requiring apical oxygen atoms that are either anionic or are hydrogen bonded to a catalytic base, including PSP, βPGM, PGK, cAPK, UMP/CMP kinase, and RhoA/RhoGAP. This is reflected by the capability of forming the TSAs, especially MgF_3^- complexes, which requires a more stringent setup in the active site of the enzyme than do fluoroaluminate complexes. Aluminum tetrafluoride has a much greater intrinsic stability in water, therefore TSAs containing it can be formed in wild-type enzymes as well as in some of their mutated variants, as long as there is at least an anionic carboxylate as apical ligand. The trifluoroberyllate ground state analogs (GSAs) that have been tested only attach to an anionic oxygen from a carboxylate or a phosphate in all of these cases. The more novel scandium and gallium species provide complexes with K-edges accessible at synchrotron beamlines, allowing unambiguous identification of

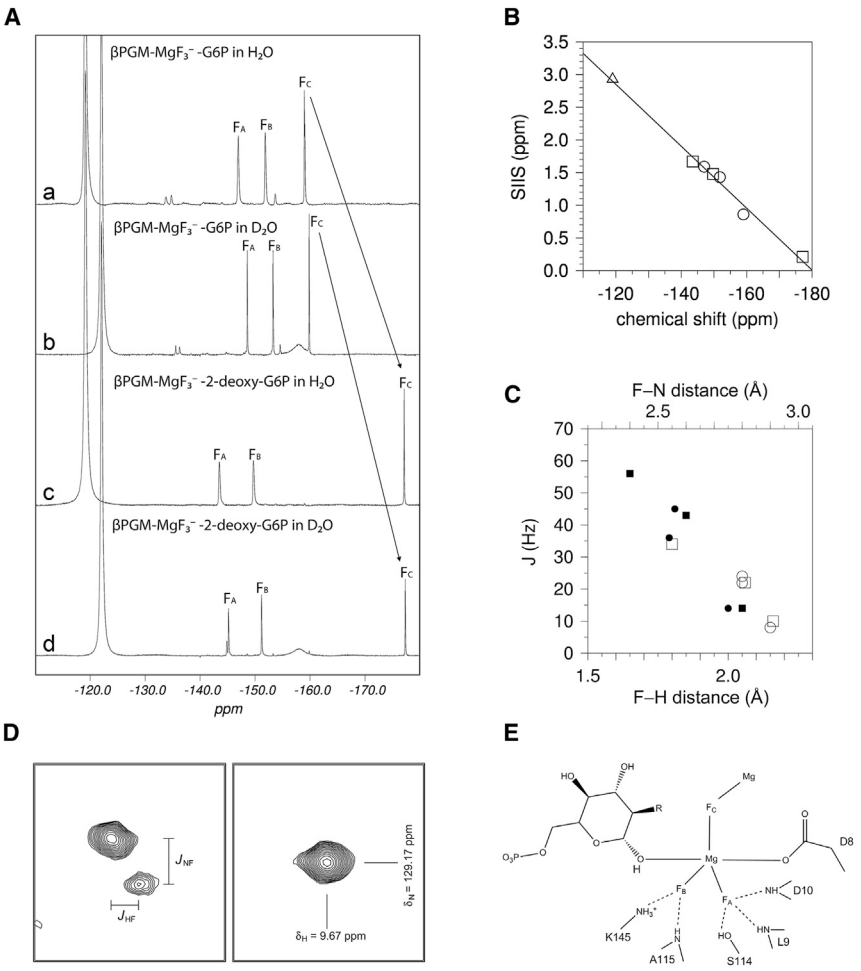

Figure 5. ^{19}F NMR parameters of metal fluorides

(A) ^{19}F NMR spectra of βPGM-MgF_3^- TSA complexes recorded at 25°C in either 50 mM HEPES 100% H_2O or 100% D_2O buffer, pH 7.2 with (a) G6P in H_2O buffer (F_A = −147.0, F_B = −151.8, F_C = −159.0 ppm), (b) G6P in D_2O buffer (F_A = −148.6, F_B = −153.3, F_C = −159.8 ppm), c) 2-deoxy-G6P in H_2O buffer (F_A = −143.5, F_B = −149.7, F_C = −177.1 ppm) and (d) 2-deoxy-G6P in D_2O buffer (F_A = −145.2, F_B = −151.2, F_C = −177.3 ppm). Free F^- resonates at −119.0 ppm in 100% H_2O buffer and at −122.0 ppm in 100% D_2O buffer. Arrows indicate the 18 ppm shift in F_C upon substrate change.

(B) Correlation plot showing the relationship between chemical shift (ppm) in H_2O buffer and SIIS (ppm) for the ^{19}F resonance of free F^- (triangle) and those of the βPGM-MgF_3^--G6P TSA complex (circles) and the βPGM-MgF_3^--2-deoxy-G6P TSA complex (squares). Linear regression analysis gives R^2 = 0.991.

(C) Correlation plot showing the relationships between $^1J_{HF}$ (filled symbols) and $^2J_{NF}$ (open symbols) couplings with the corresponding internuclear distances derived from structures of the βPGM-MgF_3^--G6P TSA (PDB 2WF5, circles) and the βPGM-AlF_4^--G6P TSA (PDB 2WF6, squares) complexes. The F-N distances are derived directly from the experimental coordinates and the F-H distances are determined to hydrogen atoms positioned using the program XPLOR.[62]

(D) Identical regions of ^{1}H, ^{15}N HSQC spectra recorded without (left) and with (right) ^{19}F decoupling showing the backbone amide resonance of A115 in the βPGM-MgF_3^--G6P TSA complex. In the left spectrum, the HN peak is split horizontally by the ^{1}H-^{19}F coupling ($^1J_{HF}$ = 36 Hz) and vertically by the ^{15}N-^{19}F coupling ($^2J_{NF}$ = 24 Hz) through the hydrogen bond to F_B of the MgF_3^- moiety. In the right spectrum, these *J*-coupling patterns collapse to an average position in a ^{1}H, ^{15}N HSQC spectrum recorded with ^{19}F decoupling in both ^{15}N and ^{1}H dimensions.

(E) Schematic view of the βPGM-MgF_3^--sugar phosphate TSA complex active site. In the βPGM-MgF_3^--G6P TSA complex (R = OH) there is a hydrogen bond between the 2-hydroxyl group of G6P and F_C of the MgF_3^- moiety. This ^{19}F resonance is significantly shifted upfield by 18.1 ppm in the βPGM-MgF_3^--2-deoxy-G6P TSA complex (R = H) in H_2O buffer as there is no corresponding hydrogen bond present.

binding sites and potential phasing applications. Metal fluorides have multiple uses, from stabilizing large complexes to the study the intricate details of catalysis and continue to be essential tools in the analysis of phosphoryl transfer enzymes in modern structural biology.

STAR★METHODS

Detailed methods are provided in the online version of this paper and include the following:

- KEY RESOURCES TABLE
- RESOURCE AVAILABILITY
  - Lead contact
  - Materials availability
  - Data and code availability
- EXPERIMENTAL MODEL AND STUDY PARTICIPANT DETAILS
- METHOD DETAILS
  - NMR methods
  - Crystallization methods
- QUANTIFICATION AND STATISTICAL ANALYSIS

SUPPLEMENTAL INFORMATION

Supplemental information can be found online at https://doi.org/10.1016/j.str.2024.07.007.

ACKNOWLEDGMENTS

The BBSRC, UK and EMBL are thanked for financial support. This work used the platforms of the Grenoble Instruct-ERIC center (ISBG; UAR 3518 CNRS-CEA-UGA-EMBL) within the Grenoble Partnership for Structural Biology (PSB), supported by FRISBI (ANR-10-INBS-0005-02) and GRAL, and financed within the Université Grenoble Alpes graduate school (Écoles Universitaires de Recherche) CBH-EUR-GS (ANR-17-EURE-0003). We acknowledge the European Synchrotron Radiation Facility for the provision of synchrotron radiation facilities, and we would like to thank the staff of the ESRF and EMBL Grenoble for assistance and support in using beamlines ID14-2, ID29, and BM29.

AUTHOR CONTRIBUTIONS

E.P., P.J., J.v.V., and M.W.B. determined optimized conditions for metal fluoride preparation in cryo-EM, SAXS, and X-ray crystallography and crystallized and determined the X-ray crystal structures of PGK and βPGM. N.J.B.,

H.R.W.D., Y.J., M.J.C., and J.P.W. performed NMR experiments. M.W.B. drafted the manuscript. J.P.W. and M.W.B. supervised the project. All authors contributed to the writing and editing of the manuscript.

DECLARATION OF INTERESTS

The authors declare no competing interests.

Received: March 25, 2024
Revised: May 24, 2024
Accepted: July 10, 2024
Published: August 5, 2024

REFERENCES

1. Bowler, M.W., Cliff, M.J., Waltho, J.P., and Blackburn, G.M. (2010). Why did Nature select phosphate for its dominant roles in biology? New J. Chem. *34*, 784–794. https://doi.org/10.1039/B9nj00718k.
2. Manning, G., Whyte, D.B., Martinez, R., Hunter, T., and Sudarsanam, S. (2002). The protein kinase complement of the human genome. Science *298*, 1912–1934. https://doi.org/10.1126/science.1075762.
3. Sternweis, P.C., and Gilman, A.G. (1982). Aluminum: a requirement for activation of the regulatory component of adenylate cyclase by fluoride. Proc. Natl. Acad. Sci. USA *79*, 4888–4891.
4. Sondek, J., Lambright, D.G., Noel, J.P., Hamm, H.E., and Sigler, P.B. (1994). GTPase mechanism of Gproteins from the 1.7-A crystal structure of transducin alpha-GDP-AIF-4. Nature *372*, 276–279. https://doi.org/10.1038/372276a0.
5. Coleman, D.E., Berghuis, A.M., Lee, E., Linder, M.E., Gilman, A.G., and Sprang, S.R. (1994). Structures of active conformations of Gi alpha 1 and the mechanism of GTP hydrolysis. Science *265*, 1405–1412.
6. Menz, R.I., Walker, J.E., and Leslie, A.G.W. (2001). Structure of bovine mitochondrial F_1-ATPase with nucleotide bound to all three catalytic sites: implications for the mechanism of rotary catalysis. Cell *106*, 331–341.
7. Rittinger, K., Walker, P.A., Eccleston, J.F., Smerdon, S.J., and Gamblin, S.J. (1997). Structure at 1.65 A of RhoA and its GTPase-activating protein in complex with a transition-state analogue. Nature *389*, 758–762. https://doi.org/10.1038/39651.
8. Scheffzek, K., Ahmadian, M.R., Kabsch, W., Wiesmuller, L., Lautwein, A., Schmitz, F., and Wittinghofer, A. (1997). The Ras-RasGAP complex: structural basis for GTPase activation and its loss in oncogenic Ras mutants. Science *277*, 333–338.
9. Schindelin, H., Kisker, C., Schlessman, J.L., Howard, J.B., and Rees, D.C. (1997). Structure of ADP x AlF4(-)-stabilized nitrogenase complex and its implications for signal transduction. Nature *387*, 370–376. https://doi.org/10.1038/387370a0.
10. Graham, D.L., Lowe, P.N., Grime, G.W., Marsh, M., Rittinger, K., Smerdon, S.J., Gamblin, S.J., and Eccleston, J.F. (2002). MgF_3^- as a transition state analog of phosphoryl transfer. Chem. Biol. *9*, 375–381.
11. Bigay, J., Deterre, P., Pfister, C., and Chabre, M. (1987). Fluoride complexes of aluminium or beryllium act on G-proteins as reversibly bound analogues of the gamma phosphate of GTP. EMBO J. *6*, 2907–2913.
12. Cho, H., Wang, W., Kim, R., Yokota, H., Damo, S., Kim, S.H., Wemmer, D., Kustu, S., and Yan, D. (2001). BeF(3)(-) acts as a phosphate analog in proteins phosphorylated on aspartate: structure of a BeF(3)(-) complex with phosphoserine phosphatase. Proc. Natl. Acad. Sci. USA *98*, 8525–8530. https://doi.org/10.1073/pnas.131213698.
13. Lee, S.Y., Cho, H.S., Pelton, J.G., Yan, D., Berry, E.A., and Wemmer, D.E. (2001). Crystal structure of activated CheY. Comparison with other activated receiver domains. J. Biol. Chem. *276*, 16425–16431. https://doi.org/10.1074/jbc.M101002200.
14. Lee, S.Y., Cho, H.S., Pelton, J.G., Yan, D., Henderson, R.K., King, D.S., Huang, L., Kustu, S., Berry, E.A., and Wemmer, D.E. (2001). Crystal structure of an activated response regulator bound to its target. Nat. Struct. Biol. *8*, 52–56. https://doi.org/10.1038/83053.
15. Yan, D., Cho, H.S., Hastings, C.A., Igo, M.M., Lee, S.Y., Pelton, J.G., Stewart, V., Wemmer, D.E., and Kustu, S. (1999). Beryllofluoride mimics phosphorylation of NtrC and other bacterial response regulators. Proc. Natl. Acad. Sci. USA *96*, 14789–14794.
16. Jin, Y., Richards, N.G., Waltho, J.P., and Blackburn, G.M. (2017). Metal Fluorides as Analogues for Studies on Phosphoryl Transfer Enzymes. Angew. Chem., Int. Ed. Engl. *56*, 4110–4128. https://doi.org/10.1002/anie.201606474.
17. Rahm, M., Hoffmann, R., and Ashcroft, N.W. (2016). Atomic and Ionic Radii of Elements 1–96. Chem. Eur J. *22*, 14625–14632. https://doi.org/10.1002/chem.201602949.
18. Shannon, R. (1976). Revised effective ionic radii and systematic studies of interatomic distances in halides and chalcogenides. Acta Crystallogr., Sect. A *32*, 751–767. https://doi.org/10.1107/S0567739476001551.
19. Cliff, M.J., Bowler, M.W., Varga, A., Marston, J.P., Szabó, J., Hounslow, A.M., Baxter, N.J., Blackburn, G.M., Vas, M., and Waltho, J.P. (2010). Transition state analogue structures of human phosphoglycerate kinase establish the importance of charge balance in catalysis. J. Am. Chem. Soc. *132*, 6507–6516.
20. Kowalinski, E., Lunardi, T., McCarthy, A.A., Louber, J., Brunel, J., Grigorov, B., Gerlier, D., and Cusack, S. (2011). Structural basis for the activation of innate immune pattern-recognition receptor RIG-I by viral RNA. Cell *147*, 423–435. https://doi.org/10.1016/j.cell.2011.09.039.
21. Uchikawa, E., Lethier, M., Malet, H., Brunel, J., Gerlier, D., and Cusack, S. (2016). Structural Analysis of dsRNA Binding to Anti-viral Pattern Recognition Receptors LGP2 and MDA5. Mol. Cell *62*, 586–602. https://doi.org/10.1016/j.molcel.2016.04.021.
22. Estévez-Gallego, J., Josa-Prado, F., Ku, S., Buey, R.M., Balaguer, F.A., Prota, A.E., Lucena-Agell, D., Kamma-Lorger, C., Yagi, T., Iwamoto, H., et al. (2020). Structural model for differential cap maturation at growing microtubule ends. Elife *9*, e50155. https://doi.org/10.7554/eLife.50155.
23. Ren, Z., Zhang, Y., Zhang, Y., He, Y., Du, P., Wang, Z., Sun, F., and Ren, H. (2019). Cryo-EM Structure of Actin Filaments from Zea mays Pollen. Plant Cell *31*, 2855–2867. https://doi.org/10.1105/tpc.18.00973.
24. Zerrad, L., Merli, A., Schroder, G.F., Varga, A., Graczer, E., Pernot, P., Round, A., Vas, M., and Bowler, M.W. (2011). A spring-loaded release mechanism regulates domain movement and catalysis in phosphoglycerate kinase. J. Biol. Chem. *286*, 14040–14048. https://doi.org/10.1074/jbc.M110.206813.
25. Baxter, N.J., Blackburn, G.M., Marston, J.P., Hounslow, A.M., Cliff, M.J., Bermel, W., Williams, N.H., Hollfelder, F., Wemmer, D.E., and Waltho, J.P. (2008). Anionic charge is prioritized over geometry in aluminum and magnesium fluoride transition state analogs of phosphoryl transfer enzymes. J. Am. Chem. Soc. *130*, 3952–3958. https://doi.org/10.1021/ja078000n.
26. Schlichting, I., and Reinstein, J. (1999). pH influences fluoride coordination number of the AlFx phosphoryl transfer transition state analog. Nat. Struct. Biol. *6*, 721–723. https://doi.org/10.1038/11485.
27. Fovet, Y., and Gal, J.-Y. (2000). Formation constants beta(2) of calcium and magnesium fluorides at 25 degrees C. Talanta *53*, 617–626. https://doi.org/10.1016/S0039-9140(00)00537-3.
28. Cui, H., Müller, A.U., Leibundgut, M., Tian, J., Ban, N., and Weber-Ban, E. (2021). Structures of prokaryotic ubiquitin-like protein Pup in complex with depupylase Dop reveal the mechanism of catalytic phosphate formation. Nat. Commun. *12*, 6635. https://doi.org/10.1038/s41467-021-26848-x.
29. Ge, M., Molt, R.W., Jr., Jenkins, H.T., Blackburn, G.M., Jin, Y., and Antson, A.A. (2021). Octahedral Trifluoromagnesate, an Anomalous Metal Fluoride Species, Stabilizes the Transition State in a Biological Motor. ACS Catal. *11*, 2769–2773. https://doi.org/10.1021/acscatal.0c04500.
30. Toyoshima, C., Nomura, H., and Tsuda, T. (2004). Lumenal gating mechanism revealed in calcium pump crystal structures with phosphate analogues. Nature *432*, 361–368. https://doi.org/10.1038/nature02981.
31. Griffin, J.L., Bowler, M.W., Baxter, N.J., Leigh, K.N., Dannatt, H.R., Hounslow, A.M., Blackburn, G.M., Webster, C.E., Cliff, M.J., and Waltho, J.P. (2012). Near attack conformers dominate beta-phosphoglucomutase

complexes where geometry and charge distribution reflect those of substrate. Proc. Natl. Acad. Sci. USA *109*, 6910–6915. https://doi.org/10.1073/pnas.1116855109.

32. Mesmer, R.E., and Baes, C.F., Jr. (1969). Fluoride complexes of beryllium(II) in aqueous media. Inorg. Chem. *8*, 618–626. https://doi.org/10.1021/ic50073a042.

33. Diaz, J.F., Sillen, A., and Engelborghs, Y. (1997). Equilibrium and Kinetic Study of the Conformational Transition toward the Active State of p21Ha-ras, Induced by the Binding of BeF3− to the GDP-bound State, in the Absence of GTPase-activating Proteins. J. Biol. Chem. *272*, 23138–23143. https://doi.org/10.1074/jbc.272.37.23138.

34. Baxter, N.J., Bowler, M.W., Alizadeh, T., Cliff, M.J., Hounslow, A.M., Wu, B., Berkowitz, D.B., Williams, N.H., Blackburn, G.M., and Waltho, J.P. (2010). Atomic details of near-transition state conformers for enzyme phosphoryl transfer revealed by MgF_3^- rather than by phosphoranes. Proc. Natl. Acad. Sci. USA *107*, 4555–4560. https://doi.org/10.1073/pnas.0910333106.

35. Baxter, N.J., Hounslow, A.M., Bowler, M.W., Williams, N.H., Blackburn, G.M., and Waltho, J.P. (2009). MgF_3^- and alpha-galactose 1-phosphate in the active site of beta-phosphoglucomutase form a transition state analogue of phosphoryl transfer. J. Am. Chem. Soc. *131*, 16334–16335. https://doi.org/10.1021/ja905972m.

36. Baxter, N.J., Olguin, L.F., Golicnik, M., Feng, G., Hounslow, A.M., Bermel, W., Blackburn, G.M., Hollfelder, F., Waltho, J.P., and Williams, N.H. (2006). A Trojan horse transition state analogue generated by MgF_3^- formation in an enzyme active site. Proc. Natl. Acad. Sci. USA *103*, 14732–14737. https://doi.org/10.1073/pnas.0604448103.

37. Ampaw, A., Carroll, M., von Velsen, J., Bhattasali, D., Cohen, A., Bowler, M.W., and Jakeman, D.L. (2017). Observing enzyme ternary transition state analogue complexes by (19)F NMR spectroscopy. Chem. Sci. *8*, 8427–8434. https://doi.org/10.1039/c7sc04204c.

38. Bowler, M.W. (2013). Conformational dynamics in phosphoglycerate kinase, an open and shut case? FEBS Lett. *587*, 1878–1883. https://doi.org/10.1016/j.febslet.2013.05.012.

39. Lallemand, P., Chaloin, L., Roy, B., Barman, T., Bowler, M.W., and Lionne, C. (2011). Interaction of human 3-phosphoglycerate kinase with its two substrates: is substrate antagonism a kinetic advantage? J. Mol. Biol. *409*, 742–757. https://doi.org/10.1016/j.jmb.2011.04.048.

40. Bruce Martin, R. (1996). Ternary complexes of Al3+ and F− with a third ligand. Coord. Chem. Rev. *149*, 23–32. https://doi.org/10.1016/S0010-8545(96)90008-9.

41. Juyoux, P., Galdadas, I., Gobbo, D., von Velsen, J., Pelosse, M., Tully, M., Vadas, O., Gervasio, F.L., Pellegrini, E., and Bowler, M.W. (2023). Architecture of the MKK6-p38α complex defines the basis of MAPK specificity and activation. Science *381*, 1217–1225. https://doi.org/10.1126/science.add7859.

42. Szilágyi, A.N., Ghosh, M., Garman, E., and Vas, M. (2001). A 1.8 A resolution structure of pig muscle 3-phosphoglycerate kinase with bound MgADP and 3-phosphoglycerate in open conformation: new insight into the role of the nucleotide in domain closure. J. Mol. Biol. *306*, 499–511. https://doi.org/10.1006/jmbi.2000.4294S0022-2836(00)94294-3.

43. Bernstein, B.E., Michels, P.A.M., and Hol, W.G.J. (1997). Synergistic effects of substrate-induced conformational changes in phosphoglycerate kinase activation. Nature *385*, 275–278. https://doi.org/10.1038/385275a0.

44. Celie, P.H.N., Toebes, M., Rodenko, B., Ovaa, H., Perrakis, A., and Schumacher, T.N.M. (2009). UV-Induced Ligand Exchange in MHC Class I Protein Crystals. J. Am. Chem. Soc. *131*, 12298–12304. https://doi.org/10.1021/ja9037559.

45. Evdokimov, A.G., Pokross, M., Walter, R., Mekel, M., Cox, B., Li, C., Bechard, R., Genbauffe, F., Andrews, R., Diven, C., et al. (2006). Engineering the catalytic domain of human protein tyrosine phosphatase beta for structure-based drug discovery. Acta Crystallogr. D *62*, 1435–1445. https://doi.org/10.1107/S0907444906037784.

46. Kontopidis, G., Andrews, M.J.I., McInnes, C., Cowan, A., Powers, H., Innes, L., Plater, A., Griffiths, G., Paterson, D., Zheleva, D.I., et al. (2003). Insights into Cyclin Groove Recognition: Complex Crystal Structures and Inhibitor Design through Ligand Exchange. Structure *11*, 1537–1546. https://doi.org/10.1016/j.str.2003.11.006.

47. Naber, N., Matuska, M., Sablin, E.P., Pate, E., and Cooke, R. (1995). A novel adenosine triphosphate analog with a heavy atom to target the nucleotide binding site of proteins. Protein Sci. *4*, 1824–1831. https://doi.org/10.1002/pro.5560040917.

48. Yount, R.G., Babcock, D., Ballantyne, W., and Ojala, D. (1971). Adenylyl imidodiphosphate, an adenosine triphosphate analog containing a P-N-P linkage. Biochemistry *10*, 2484–2489. https://doi.org/10.1021/bi00789a009.

49. Gruen, M., Becker, C., Beste, A., Reinstein, J., Scheidig, A.J., and Goody, R.S. (1999). 2'Halo-ATP and -GTP analogues: rational phasing tools for protein crystallography. Protein Sci. *8*, 2524–2528. https://doi.org/10.1110/ps.8.11.2524.

50. Carrasco, N., Ginsburg, D., Du, Q., and Huang, Z. (2001). Synthesis of selenium-derivatized nucleosides and oligonucleotides for X-ray crystallography. Nucleos Nucleot. Nucleic Acids *20*, 1723–1734. https://doi.org/10.1081/ncn-100105907.

51. Munoz, I.G., Yébenes, H., Zhou, M., Mesa, P., Serna, M., Park, A.Y., Bragado-Nilsson, E., Beloso, A., de Carcer, G., Malumbres, M., et al. (2011). Crystal structure of the open conformation of the mammalian chaperonin CCT in complex with tubulin. Nat. Struct. Mol. Biol. *18*, 14–19. https://doi.org/10.1038/nsmb.1971.

52. Dawson, R.J., and Locher, K.P. (2006). Structure of a bacterial multidrug ABC transporter. Nature *443*, 180–185. https://doi.org/10.1038/nature05155.

53. Park, S., Ajtai, K., and Burghardt, T.P. (1999). Inhibition of myosin ATPase by metal fluoride complexes. Biochim. Biophys. Acta *1430*, 127–140.

54. Danielson, M.A., and Falke, J.J. (1996). Use of 19F NMR to probe protein structure and conformational changes. Annu. Rev. Biophys. Biomol. Struct. *25*, 163–195. https://doi.org/10.1146/annurev.bb.25.060196.001115.

55. Gerig, J.T. (1989). Fluorine nuclear magnetic resonance of fluorinated ligands. Methods Enzymol. *177*, 3–23.

56. Spotswood, T., Evans, J.M., and Richards, J.H. (1967). Enzyme–substrate interaction by nuclear magnetic resonance. J. Am. Chem. Soc. *89*, 5052–5054.

57. Oldfield, E. (2005). Quantum chemical studies of protein structure. Philos. Trans. R. Soc. Lond. B Biol. Sci. *360*, 1347–1361. https://doi.org/10.1098/rstb.2003.1421.

58. Koudelka, G.B., Hansen, F.B., and Ettinger, M.J. (1985). Solvent isotope effects and the pH dependence of laccase activity under steady-state conditions. J. Biol. Chem. *260*, 15561–15565.

59. Bernheim, R.A., and Batiz-Hernandez, H. (1964). Indirect Nuclear Spin—Spin Coupling and Isotope Shifts in the Nuclear Magnetic Resonance of 15NH3, 15NH2D, and 15NHD2. J. Chem. Phys. *40*, 3446–3447. https://doi.org/10.1063/1.1725029.

60. Kanazawa, Y., Baldeschwieler, J.D., and Craig, N.C. (1965). NMR and double resonance spectra of the deuterodifluoroethylenes. J. Mol. Spectrosc. *16*, 325–348. https://doi.org/10.1016/0022-2852(65)90128-1.

61. Wood, H.P., Cruz-Navarrete, F.A., Baxter, N.J., Trevitt, C.R., Robertson, A.J., Dix, S.R., Hounslow, A.M., Cliff, M.J., and Waltho, J.P. (2020). Allomorphy as a mechanism of post-translational control of enzyme activity. Nat. Commun. *11*, 5538. https://doi.org/10.1038/s41467-020-19215-9.

62. Brunger, A.T. (1992). XPLOR: A System for X-Ray Crystallography and NMR (Yale University Press).

63. Flachner, B., Varga, A., Szabó, J., Barna, L., Hajdú, I., Gyimesi, G., Závodszky, P., and Vas, M. (2005). Substrate-Assisted Movement of the Catalytic Lys 215 during Domain Closure: Site-Directed Mutagenesis

Studies of Human 3-Phosphoglycerate Kinase. Biochemistry *44*, 16853–16865. https://doi.org/10.1021/bi051726g.

64. Leslie, A.G.W. (1992). Recent changes to the MOSFLM package for processing film and image plate data. In Joint CCP4 and EACMB Newsletter on Protein Crystallography 26, Warrington: Daresbury Laboratory.
65. Collaborative Computational Project Number 4 (1994). The CCP4 suite: programs for protein crystallography. Acta Cryst. D Biol. Cryst. *50*, 760–763.
66. Adams, P.D., Afonine, P.V., Bunkoczi, G., Chen, V.B., Davis, I.W., Echols, N., Headd, J.J., Hung, L.-W., Kapral, G.J., Grosse-Kunstleve, R.W., et al. (2010). PHENIX: a comprehensive Python-based system for macromolecular structure solution. Acta Crystallogr. D *66*, 213–221. https://doi.org/10.1107/S0907444909052925.
67. Emsley, P., and Cowtan, K. (2004). Coot: model-building tools for molecular graphics. Acta Crystallogr. D *60*, 2126–2132.
68. Pellegrini, E., Piano, D., and Bowler, M.W. (2011). Direct cryocooling of naked crystals: are cryoprotection agents always necessary? Acta Crystallogr. D Biol. Crystallogr. *67*, 902–906. https://doi.org/10.1107/S0907444911031210.
69. Svensson, O., Gilski, M., Nurizzo, D., and Bowler, M.W. (2018). Multi-position data collection and dynamic beam sizing: recent improvements to the automatic data-collection algorithms on MASSIF-1. Acta Crystallogr. D Struct. Biol. *74*, 433–440. https://doi.org/10.1107/S2059798318003728.
70. Svensson, O., Malbet-Monaco, S., Popov, A., Nurizzo, D., and Bowler, M.W. (2015). Fully automatic characterization and data collection from crystals of biological macromolecules. Acta Crystallogr. D *71*, 1757–1767. https://doi.org/10.1107/S1399004715011918.
71. Vagin, A., and Teplyakov, A. (1997). MOLREP: an automated program for molecular replacement. J. Appl. Crystallogr. *30*, 1022–1025.
72. Murshudov, G.N., Vagin, A.A., and Dodson, E.J. (1997). Refinement of macromolecular structures by the maximum-likelihood method. Acta Cryst. D Biol. Cryst. *53*, 240–255.
73. Gabadinho, J., Beteva, A., Guijarro, M., Rey-Bakaikoa, V., Spruce, D., Bowler, M.W., Brockhauser, S., Flot, D., Gordon, E.J., Hall, D.R., et al. (2010). MxCuBE: a synchrotron beamline control environment customized for macromolecular crystallography experiments. J. Synchrotron Radiat. *17*, 700–707. https://doi.org/10.1107/S0909049510020005.

Please cite this article in press as: Pellegrini et al., Metal fluorides—multi-functional tools for the study of phosphoryl transfer enzymes, a practical guide, Structure (2024), https://doi.org/10.1016/j.str.2024.07.007

STAR★METHODS

KEY RESOURCES TABLE

REAGENT or RESOURCE	SOURCE	IDENTIFIER
Chemicals, peptides, and recombinant proteins		
Aluminium chloride	Sigma-Aldrich	206911
Magnesium chloride	Sigma-Aldrich	M2670
Beryllium chloride	Sigma-Aldrich	201197
Scandium chloride	Sigma-Aldrich	409359
Gallium chloride	Sigma-Aldrich	427128
ADP	Sigma-Aldrich	A2754
AMP-PCP	Sigma-Aldrich	M7510
Deferoxamine	Sigma-Aldrich	D9533
Ammonium fluoride	Sigma-Aldrich	338869
sodium fluoride	Sigma-Aldrich	S1504
3-phosphoglycerate	Sigma-Aldrich	P8877
Glucose-6-phosphate	Sigma-Aldrich	G7250
2-deoxyglucose-6-phosphate	Sigma-Aldrich	SMB00932
Deposited data		
Structure factors and coordinates of the PGK-ADP-3PG complex	This paper	PDB 2X13
Structure factors and coordinates of the PGK(K219A)-AMPPCP-3PG complex	This paper	PDB 2X14
Structure factors and coordinates of the PGK-ADP-BeF_3^--3PG complex	This paper	PDB 4AXX
Structure factors and coordinates of the βPGM-ScF_4^--G6P TSA complex	This paper	PDB 3ZI4
Software and algorithms		
MXCuBE data collection software	Gabadinho et al.[73]	https://mxcube.github.io/mxcube/
Workflows for sample centring and data collection	Svensson et al.[69,70]	https://ewoksmx.readthedocs.io/
Mosflm	Leslie[64]	https://www.mrc-lmb.cam.ac.uk/harry/imosflm/ver740/introduction.html
Phenix	Adams et al.[66]	https://phenix-online.org/
CCP4	CCP4 et al.[65]	https://www.ccp4.ac.uk/
COOT	Emsley and Cowtan[67]	https://www2.mrc-lmb.cam.ac.uk/personal/pemsley/coot/
Pymol	The PyMOL Molecular Graphics System, Version 3.0 Schrödinger, L	https://pymol.org/
FELIX	Felix NMR, Inc., San Diego, CA	http://www.felixnmr.com/
XPLOR	Brunger, A.T.[62]	https://nmr.cit.nih.gov/xplor-nih/xplorMan/

RESOURCE AVAILABILITY

Lead contact

Further information and requests for resources and reagents should be directed to and will be fulfilled by the lead contact, Matthew Bowler (mbowler@embl.fr).

Materials availability

This study did not generate new unique reagents.

Please cite this article in press as: Pellegrini et al., Metal fluorides—multi-functional tools for the study of phosphoryl transfer enzymes, a practical guide, Structure (2024), https://doi.org/10.1016/j.str.2024.07.007

Data and code availability

- The coordinates and structure factors have been deposited in the Protein Data Bank (PDB) under the following accession codes 2X13 for the PGK-ADP-3PG complex, 2X14 for the PGK(K219A)-AMPPCP-3PG complex and 4AXX for the PGK-ADP-BeF_3^--3PG complex; and 3ZI4 for the βPGM-ScF_4^--G6P TSA complex and are publicly available as of the date of publication. These accession numbers are also listed in the key resources table.
- This paper does not report any original code.
- Any additional information required to reanalyze the data reported in this paper is available from the lead contact upon request.

EXPERIMENTAL MODEL AND STUDY PARTICIPANT DETAILS

DH5α *E. coli* cells were grown at 37°C in LB media for cloning.

BL21(DE3) Codon plus RIL *E. coli* cells were grown at 37°C in LB supplemented with Kanamycin or Ampicillin and protein expression was induced with IPTG at 37°C.

BL21(DE3) *E. coli* cells were grown at 37°C in LB supplemented with kanamycin or ampicillin and protein expression was induced with IPTG at 37°C.

METHOD DETAILS

NMR methods

All ^{19}F NMR experiments were recorded at 298 K on a Bruker Avance 500 MHz spectrometer (operating at 470.38 MHz for ^{19}F) equipped with a QXI ($^{1}H/^{13}C/^{15}N/^{19}F$) probe. Typically, ~64k transients were acquired without ^{1}H decoupling over a spectral width of 100 ppm and were processed using FELIX (Felix NMR, Inc., San Diego, CA) with backward linear prediction and sinebell functions shifted by 60°. All samples contained 1 mM β-PGM, 5 mM $MgCl_2$, 10 mM NaF, 10 mM G6P and 2 mM NaN_3 as a preservative, in HEPES buffer prepared in 100% D_2O at pH 7.2 except for the GaF_4^- complex which was recorded at pH 6.0 (Ga^{3+} ions precipitate as $Ga(OH)_3$ at pH values above 6.0). The βPGM-AlF_4^--G6P complex was supplemented with 3 mM $AlCl_3$, whereas the βPGM-ScF_4^--G6P and the βPGM-GaF_4^--G6P complexes were recorded using 10 mM of the appropriate metal chloride, which was necessary to out-compete the βPGM-MgF_3^--G6P complex in both cases. Out of 10 metals screened (Ca, Sc, Co, Ni, Cu, Zn, Ga, Ge, Sr and Y) we found that only scandium (III) and gallium (III) were able to form metal fluoride complexes with βPGM (Figure 3A).

Crystallization methods

PGK

Human wild type PGK was cloned into a pET11c vector and expressed in *E. coli*, as previously described.[19,24,63] Briefly, PGK was overexpressed in *E. coli* BL21-CodonPlus (DE3)-RIL cells (Stratagene), purified by ammonium sulfate precipitation and CM-Sepharose chromatography. Attempts to co-crystallize PGK in the closed conformation with ADP, AMP-PCP, or BeF_3^- failed. Therefore, crystals of the MgF_3^- and AlF_4^- TSA complexes were subjected to cross soaks to obtain these complexes as follows: Crystals of the PGK-3PG-MgF_3^--ADP (2WZC), the PGK-3PG-AlF_4^--ADP (2WZB) and the PGK(K219A)-3PG-AlF_3^--ADP (2WZD) complexes were obtained as described previously.[19,24] Briefly, lyophilized PGK was resuspended in 50 mM Tris (pH 7.5), 20 mM DTT, 25 mM $MgCl_2$, 50 mM 3PG, and 10 mM ADP. The PGK-3PG-MgF_3^--ADP TSA complex was supplemented with 20 mM NH_4F and 1 mM deferoxamine, which was included to chelate any contaminating aluminum. The PGK-3PG-AlF_4^--ADP TSA and PGK(K219A)-3PG-AlF_3^--ADP complex samples were supplemented with 20 mM NH_4F and 5 mM $AlCl_3$. The final protein concentration was 15 mg mL^{-1}. Crystals with the approximate dimensions of 0.5 × 0.1 × 0.05 mm were obtained by vapor diffusion in 4 μL sitting drops of 50:50 mix of protein solution and precipitant (28−33% PEG 2000 MME and 0.1 M Bis/Tris pH 6.5). For cross-soaking crystals were transferred to cryoprotection buffers (35% PEG 2000 MME; 0.1 M Bis/Tris pH 6.5, 20 mM DTT, 25 mM $MgCl_2$ and 50 mM 3PG) lacking aluminium chloride or ammonium fluoride and containing 10 mM of the relevant nucleotide (ADP or AMP-PCP) and 0.1mM deferoxamine. For the PGK-3PG-BeF_3^--ADP structure (4AXX), the soak solution included 10 mM ADP, 10 mM NH_4F and 10 mM $BeCl_2$. For the PGK-3PG-ADP complex (2X13), PGK-3PG-MgF_3^--ADP crystals (2WZC) were soaked for 30 mins; for the PGK(K219A)-3PG-AlF_3^--AMPPCP complex (2X14), PGK(K219A)-3PG-AlF_3^--ADP (2WZD) crystals were soaked for 1 hour, and for the PGK-3PG-BeF_3^--ADP complex (4AXX), PGK-3PG-MgF_3^--ADP crystals (2WZC) were soaked for 1 hour. Soaking PGK-3PG-MgF_3^--ADP crystals (2WZC) or PGK-3PG-AlF_4^--ADP crystals (2WZB) with AMP-PCP was not successful (metal fluoride was removed but ADP remained). After soaking, the crystals were harvested, plunged into liquid nitrogen and stored at 100 K. Diffraction data were collected from cryo-cooled crystals to between 1.9 Å and 1.74 Å resolution on an ADSC Q210 CCD detector at beamline ID14-2 (λ=0.933 Å) at the European Synchrotron Radiation Facility (ESRF), Grenoble, France (see Table 1). Data were processed with MOSFLM[64] and programs from the Collaborative Computational Project Number 4 (CCP4) suite[65] or Phenix.[66] The complexes crystallised in the orthorhombic space group $P2_12_12_1$ with one molecule in the asymmetric unit. The structures were solved by molecular replacement using the PGK-3PG-MgF_3^--ADP TSA complex (PDB accession code 2WZB [19]) for the closed conformation as search models with all ligands and water molecules removed. In all subsequent refinement steps, 5% of the data were excluded for calculating the free R-factor. Refinement was carried out alternately with REFMAC5[50] or Phenix.refine,[66] and by manual rebuilding with the program COOT.[67] Ligands

were not included until the final rounds of refinement so they could be built into unbiased difference Fourier maps. Stereochemistry was assessed with COOT with all residues in preferred or allowed regions.

βPGM

The expression and purification of βPGM was performed as described previously.[36] Briefly, βPGM was cloned into a pET11b vector, expressed in *E. coli* BL21 (DE3) cells and purified using anion exchange and size exclusion chromatography. The βPGM-ScF_4^--G6P TSA complex was prepared by adding 10 mM NH_4F and 10 mM $ScCl_3$ to the protein sample, followed by 5 mM G6P and the solution adjusted to a protein concentration of 15 mg ml^{-1}. For crystallization, 2 μl of the ScF_4^- inhibited protein was mixed 1:1 with the precipitant (26-30 % (w/v) PEG 4000, 200 mM sodium acetate and 100 mM Tris pH 7.5) and placed in sitting drop crystallisation plates. Small diamond shaped plate crystals appeared overnight with the approximate dimensions 0.01 mm x 0.01 mm x 0.001 mm. Crystals were harvested on a micromesh loop (MiTeGen, Ithaca, NY) and excess mother liquor was removed before plunging into liquid nitrogen according to established protocols.[68] Diffraction data were collected from cryo-cooled crystals to 1.33 Å resolution on an ADSC Q4R CCD detector on beamline ID14-2 (λ=0.933 Å) for native data and to 1.95 Å resolution on an ADSC Q315 detector on beamline ID29 (λ=1.77 Å, E = 7 keV) for the long wavelength data set of the βPGM-ScF_4^--G6P complex, at the European Synchrotron Radiation Facility (ESRF), Grenoble, France (see Table 2) using protocols for optimized sample location and characterisation.[69,70] The complex crystallised in the orthorhombic space group $P2_12_12_1$ with one molecule in the asymmetric unit. Data were processed with MOSFLM[64] and programs from the Collaborative Computational Project Number 4 (CCP4) suite.[65] The structure was determined by molecular replacement with MolRep[71] using PDB accession code 2WF5 [34] as a search model with all ligands and water molecules removed. In all subsequent refinement steps, 5% of the data were excluded for calculating the free R-factor. Refinement was carried out alternately with REFMAC5[72] and by manual rebuilding with the program COOT.[67]

QUANTIFICATION AND STATISTICAL ANALYSIS

Crystallographic data collection and refinement statistics are shown in Tables 1 and 2.